strain
An International Journal for Experimental Mechanics

Mechanical behaviour of PVC/$CaCO_3$ Particulate Composites – Influence of Temperature

J. D. M. Costa*, C. Capela† and J. A. M. Ferreira*

*CEMUC/CDRSP, Department of Mechanical Engineering, University of Coimbra – Pólo II, 3030-788 Coimbra, Portugal

†Department of Mechanical Engineering, Polytechnic Institute of Leiria, Leiria, Portugal

ABSTRACT: This paper is concerned with the study of temperature influence on Young's modulus, ultimate strength and fracture toughness properties of PVC/$CaCO_3$ particulate composites with different volume fractions. The tests were performed in three- and four-point bending. The resonant technique was also used to analyse the influence of both volume fraction and temperature on Young's modulus. Significant decrease of ultimate strength, fracture toughness and Young's modulus was observed with the increase of the temperature. Ultimate strength decreases with the increase of particle volume fraction at room temperature. For the other temperatures, this decreasing trend is less clear. PVC/$CaCO_3$ flexural Young's modulus calculated for a much lower loading segment increases with volume fraction. The same trend was obtained using the resonant technique. However, as the loading segment used to calculate the Young's modulus was increased a significant decrease of Young's modulus was obtained as a result of a progressive debonding at the particle-matrix interface. A 2D simplified FE simulation also confirms such trend. The dependence of Young's modulus relatively to the loading segment increases as the volume fraction is increased, leading to composite Young's modulus below matrix value for higher volume fractions and higher loading segments. Fracture toughness decreases with volume fraction.

KEY WORDS: *flexural strength, fracture toughness, particulate composites, Young's modulus*

Introduction

Polymer-based composites with particles have been replacing conventional engineering materials, like cast steels or stainless steels, in a wide range of applications. The use of particles in polymer composites improves, in most cases, mechanical and thermal properties, such as the Young's modulus, creep resistance and in some cases fracture toughness. This type of composites can also lead to the reduction of its thermal expansion and to the increase of its resistance to wear. A number of parameters, such as the size, shape, aspect ratio, volume fraction and distribution of reinforcement particles, affect the composite properties [1–3]. PVC, as a commodity plastic, has been used in industrial fields for many years because of its good properties, but its low toughness and heat-softening temperature restrict its application [4].

Voros *et al.* [5], studying materials with particles filler of $CaCO_3$, has shown that the size of the particles affects the tensile strength and increases with the volume fraction when the size of the filler particles is smaller. The highest value of tensile strength is achieved with the smallest particle size. Pukanszky *et al.* [6] observed that both talcum and $CaCO_3$ lead to an increase of Young's modulus and that the addition of low strength material decreases it. On the other hand, Young's modulus variation depends upon the interaction between the filler and the matrix. Ahmed *et al.* [3] considered that the simplest form to achieve Young's modulus is by determining the limit values given by the Voigt and Reuss models [7]. The tensile strength provides information about the interaction between matrix and filler and is one of the most used parameters in the characterisation of composite materials [8–10]. Vollerberg *et al.* [10] observed that smaller particles of silica were more effective as a reinforcement of the thermoplastic matrix. Liang *et al.* [11] observed that both strength and fracture toughness increase with the addition of glass spheres in a matrix of PP. On the other hand, Moloney *et al.* [12] did not observe particle size effect in matrix epoxy resin. In a recent work, Zeng *et al.* [13] studied the effect of the diameter of $CaCO_3$ particles on the properties of polymeric blends. The results showed that the composites with the smaller nanoparticles presented the higher mechanical properties. By adding 40-nm $CaCO_3$

doi: 10.1111/j.1475-1305.2009.00624.x

nanoparticles into the PVC matrix, the single-notched impact strength of the nanocomposite at room temperature was 3.5 times that of the PVC matrix and 4.6 times that of the PVC blend filled with micro-$CaCO_3$.They also obtained a slight better performance of nanocomposites with 40- and 80-nm $CaCO_3$ particles than the composites with 500-nm and 25-μm $CaCO_3$ particles, concerning tensile and flexural properties.

Young's modulus can be determined by several techniques. A very expeditious technique is to use an experimental procedure based on the strain gauge-based resonant technique. This technique is based on the fundamental relation that exists between elastic properties of a structure and its vibratory behaviour. Resonant frequencies were determined experimentally from simple sample shapes. This technique presents the following main advantages: several elastic properties can be determined from a single specimen; the vibration of the specimen gives average values of the elastic constants; small samples can be used; it is adequate for brittle materials; it is a non-destructive technique. Several studies using this technique to determine the elastic parameters can be found in the literature [14]. A recent paper studied the accuracy of the resonant technique using an experimental–numerical procedure [15] and a great sensitivity to the geometry was found, which emphases the need for ideally shaped specimens and accurate measurements of its dimensions. The authors also concluded that bending and torsion modes are sensitive to Young's modulus and shear modulus, respectively.

This work is concerned with a study of the flexure Young's modulus, flexure resistance and fracture toughness of PVC-$CaCO_3$ particulate composites with different volume fractions. The influence of temperature on these properties was also analysed. Young's modulus was obtained with both flexure tests and resonant technique. A simplified 2D FE analysis was also performed to understand Young's modulus variations observed during flexure tests.

Materials and Experimental Procedure

The material studied in this work was PVC-based composites filled with particles composed by 99% of $CaCO_3$ and 0.55% of $MgCO_3$ with 2.5 μm of size. Some exploratory flexure tests with other particle sizes (Table 1) were also performed. Volume fraction (V_f) ranged from 0.8 to 16 %. The fillers had particles with crystalline rhombohedral shape.

An amount of 2 kg of composite material was prepared for each composition and produced in two steps. In the first step, a mixer machine Henschel TM10L (Henschel, Kassel, Germany) was used, where the matrix (PVC), the lubricants (AC-316A and GP-02) and the octyl thiotin stabiliser (OTS 17D) were mixed during approximately 12 min while the temperature was increased to 80ºC. Then the dioctyl phthalate plasticiser (7.4% in weight) was introduced, slowly, during about 4 min until a temperature of 110 °C was attained. Finally, the first step was finished with the addition of the filler and an increase in temperature up to 120 °C. The second step was the injection moulding. For this purpose prismatic specimens, as shown in Figure 1, were prepared in a cold channel type carbon steel mould, using a Buehler Rover 63B plastics injection machine (Buhler, Vezwil, Switzerland). The injection occurred during 5 s, followed by 30 s of cooling. A pressure of 10 MPa and a temperature of 185 °C were applied. Lubricants, stabiliser of suspension, plasticiser and colorants represented a total of 18.7% in weight fraction of the matrix.

Flexural strength tests were carried out with specimens presenting the geometry illustrated in Figure 1A) and using a four-point bending apparatus. Figure 1B) shows the geometry of the fracture toughness specimens as well as the three-point bending scheme used in these tests.

The tests were performed using a computer controlled Instron universal testing machine fitted with an oven for temperature control. The accuracy of the temperature control is better than 1 °C. At least three replicas were tested for each condition. The loading rate was 0.5 mm min^{-1}.

To analyse the dependence of flexural strength on temperature, the tests were conducted over a temperature range of 20–50 °C. These tests were performed at four-point bending specimens with a span ratio of 0.5. The ratio between the specimen span length (L = 60 mm) and its height (h = 8 mm) gives a slenderness ratio L/h = 7.5. Because this value seems to be too low to apply elementary beam theory without correction, a finite element analysis was

Table 1: Compositions of the materials tested

Trade name	Filler	Density	Particle size (μm)	Volume fraction (%)
PVC	–	1.317	–	–
BSH	$CaCO_3$ (99%) + $MgCO_3$ (0.55%)	1.367–1.553	2.5–30	0.8–16

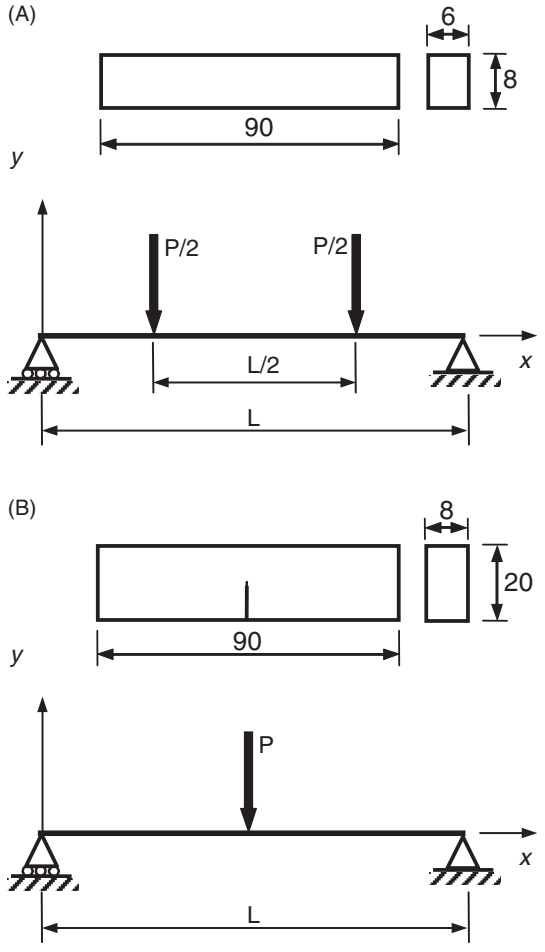

Figure 1: Specimens geometry for: (A) flexural strength four-point bending tests; (B) fracture toughness three-point bending tests. Dimensions in mm. L = 60 mm

performed to calculate flexure displacements at roller loading contacts and compare these values with elementary beam theory ones. A coefficient of correction k was calculated for three- and four-point bending specimens, ranging L/h between 5 and 22.5. The results obtained in this analysis are summarised in Table 2, presenting k for three- and four-point bending tests for each value of the slenderness ratio L/h. It was observed that for $L/h = 7.5$, k becomes a significant correction factor, taking the value of 1.052 and that for $L/h > 22.5$, elementary beam theory can be applied without correction ($k = 1$). Therefore, using the elasticity theory and the coefficient k for slenderness correction, δ can be related with the applied load P, geometric parameters and the flexural Young modulus E through Equation (1)

$$\delta = \frac{kPL^3}{96EI} \tag{1}$$

where I is the bending inertia momentum of the transversal section and L is the span length indicated in Figure 1. The displacement δ was measured at the roller/specimen contact points. The meaning of E in Equation (1) can be made explicit in the form

$$E = \frac{kP}{\delta} \times \frac{L^3}{96I} \tag{2}$$

The flexural Young's modulus was then calculated through Equation (2) using the higher tangent to the initial part of the P–δ experimental curves obtained in the flexural strength tests. Young's modulus for higher segments of loading, but considerably below plastic yielding, were also determined to analyse if there was a progressive stiffness loss as a result of particle–matrix debonding. These tests were performed according to the ASTM D790M-93 [16] standard.

Young's modulus was also determined using an experimental procedure based on the resonant technique. The determination of elastic constants using the resonant technique has three main steps: the experimental determination of resonant frequencies; the analytical or numerical definition of relations between resonant frequencies and elastic properties; and the determination of elastic properties. Parallelepipedic geometries are often used to determine the elastic constants of this technique. Free–free boundary conditions were used, considering its advantageous easiness to reproduce both experimentally and numerically. A thin wire was used to approximate the free boundary conditions. Mechanical excitation of natural modes was produced by impact loading using a small elastic hammer. Small loads were applied avoiding material damage and allowing test repetition on the same sample. A strain gauge with 2 mm length and 120 Ω of electrical resistance, glued to the sample, was used as a sensor to measure the mechanical vibration response of the composites. The strain gauge length was aligned with the longitudinal direction of the sample. A small size of the

Table 2: Coefficient of correction for elementary beam theory taking into account slender ratio

L/h	5	7.5	10	12.5	15	17.5	20	22.5
k (4PB)	1.137	1.052	1.021	1.015	1.008	1.004	1.002	1.000
k (3PB)	1.140	1.052	1.022	1.015	1.009	1.005	1.004	1.002

4PB, four-point bending; 3PB, three-point bending.

doi: 10.1111/j.1475-1305.2009.00624.x

strain gauge was used to produce a reduced effect on the resonant frequencies. Careful selection of strain gauge position is required to identify the resonant frequencies associated with flexural modes. The impulsive load used in impact resonance techniques activates normally all vibration modes, but the position of the extensometer(s) determines the sensitivity to measure each mode. Considering that the objective of this study was the evaluation of E, the measure was focused on the longitudinal bending modes. Therefore, to have high sensitivity to measure the three first bending modes, the extensometers were located in the longitudinally axis at a position distance of ($5L/12$) from the edge.

For isotropic materials, the analytical formulas for beam-shaped test samples are used directly to calculate the Young's modulus from experimental resonant frequencies. European and American standard test procedures ASTM E1876-01 [17] propose the following equation to calculate E along the main axis of beam like samples from the first flexural frequency:

$$E = 0.946\frac{mf^2}{W}\left(\frac{L}{t}\right)^3 A_f \quad (3)$$

f being the resonant frequency, L the length, W the width, t the thickness and A_f a shape factor [17].

The samples were cut from the flexural specimens shown in Figure 1A, being the length of the samples aligned with the longitudinal direction of the specimens. The samples were parallelepiped shaped with $7 \times 2 \times 75$ mm.

For fracture toughness evaluation, an initial crack was created in the specimens (Figure 1B) by pressing a small razor blade against a previously cut notch. These and other details of the procedures used are described in 'Testing Protocol EGF Task Group on Polymers and Composites – Protocol for K_c/G_c Standard' for polymers with a toughness below 2 MPa $\sqrt{m}$ [18]. Initial crack length was measured with an optical microscope. Load–displacement curves were obtained from load cell and clip gauge measurements. The tests were undertaken at three different temperatures: 20, 30 and 40 °C. Fracture surfaces were then scanned by an electronic microscope to observe the failure mechanisms.

Results and Discussion

Flexure tests

Figure 2 shows typical curves obtained in the flexural tests for three temperatures (20, 40 and 50 °C) in the PVC/$CaCO_3$ composites with two different volume fractions. For clarity, PVC curves were not included in Figure 2 PVC because they are almost superimposed with 1.6% volume fraction composite curves. The tests were performed as indicated in Figure 1 (flexural strength four-point bending tests and fracture toughness three-point bending tests). As expected, it was observed that the temperature significantly affects the maximum load, and the stiffness and the viscous-plastic flow of this material. As the temperature increases, the material presents a progressive increase in plasticity, typical of thermoplastic polymers. A slight decrease of the ultimate strength with increasing volume fraction was observed, which is the expected behaviour.

Figure 3 shows the variation of the ultimate strength (maximum bending stress to maximum load) with the temperature (20, 40 and 50 °C), against volume fractions for $CaCO_3$ filler with a particle size of 2.5 μm. The maximum bending stress was calculated assuming an elastic behaviour of the four-point bending specimens. A significant decrease on ultimate strength was observed with the increase of temperature, as expected. At room temperature, ultimate strength decreases with the increase of particle volume fraction. For the other temperatures, this trend is more moderate, being practically absent in T = 50 °C.

Figure 4 presents a comparison between experimental results of the ultimate stress against volume fraction and the estimations based on theoretical models for the three temperatures analysed. In general, all models preview a decrease of the tensile or flexural resistance of particle composites with the increase of the volume fraction of the filler. In the

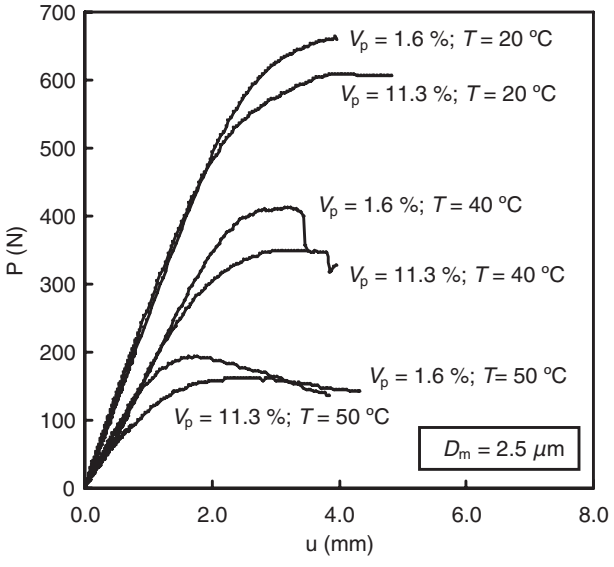

Figure 2: Load–displacements curves for different temperatures and volume fractions

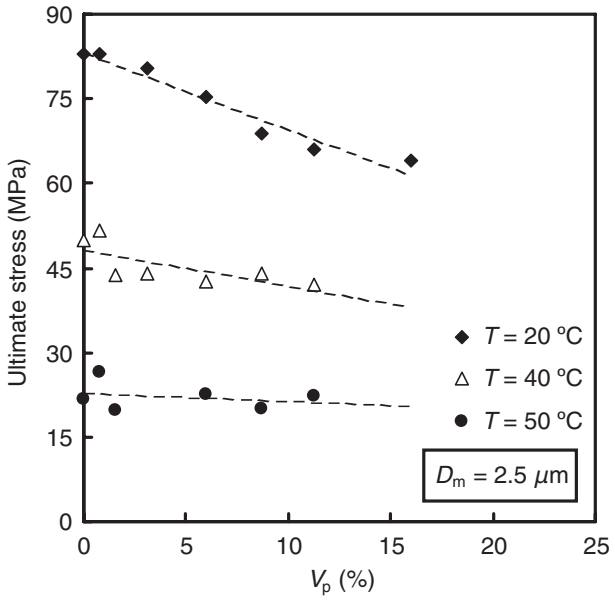

Figure 3: Ultimate stress against volume fraction for different temperatures

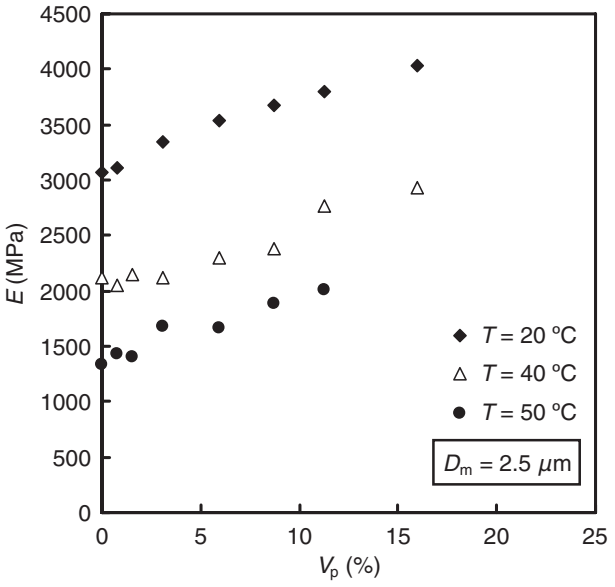

Figure 5: Young's modulus for different temperatures as function of volume fraction

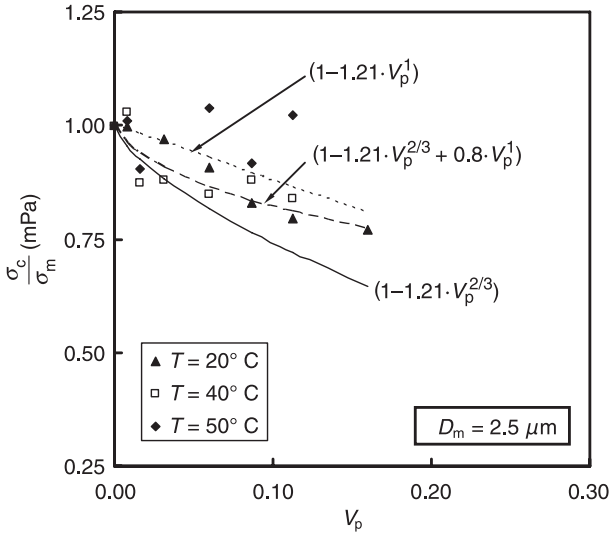

Figure 4: Comparison of the experimental results with theoretical models

case of a poor adhesion, where no or a weak stress transfer occurs between matrix and filler, a lower bound for the strength of the composite was presented by Nicolais and Nikodemo [19],

$$\sigma_c = \sigma_m\left(1 - aV_p^b\right) \tag{4}$$

where σ_c is the tensile strength of the filled composite, σ_m is the tensile strength of the polymer, a is a constant related to stress concentration (a = 1.21 for spherical particles having no adhesion) and b is a constant related to the geometry of the filler. In Figure 4, Equation (3) was plotted taking a = 1.21 and two values for the exponent b = 2/3 and 1. The results are predominantly between these two curves, except the results for T = 50 °C, which are less dependent on the addition of the filler.

An upper bound is more difficult to obtain because it depends on the level of adhesion between matrix and filler, which increases the tensile strength, and also of the competing loss in strength because of stress concentration at the polymer/filler interface. On a purely empirical basis, an extension of Equation (3) was suggested by Bigg [20],

$$\sigma_c = \sigma_m\left(1 - aV_p^b + cV_p^d\right) \tag{5}$$

where c and d are coefficients that should be indicators of polymer/filler adhesion. In Figure 4, this equation was also plotted with a = 1.21, b = 2/3, c = 0.8 and d = 1, which appear to give a good correlation with the experimental results. Other models were also tried but did not achieve a better correlation.

Figure 5 shows the variation of tangent modulus with temperature (20, 40 and 50 °C) against volume fraction for $CaCO_3$ filler with a particle size of 2.5 μm. These E-values were calculated using the higher tangent to the initial part of the P–δ experimental curves obtained in the flexural strength tests. A significant decrease on tangent modulus was observed with the increase of temperature. A monotonic increase of tangent modulus with volume fraction was observed for the three temperatures analysed, because of the higher Young's modulus of the filler. This is in agreement with the generally observed trend.

doi: 10.1111/j.1475-1305.2009.00624.x

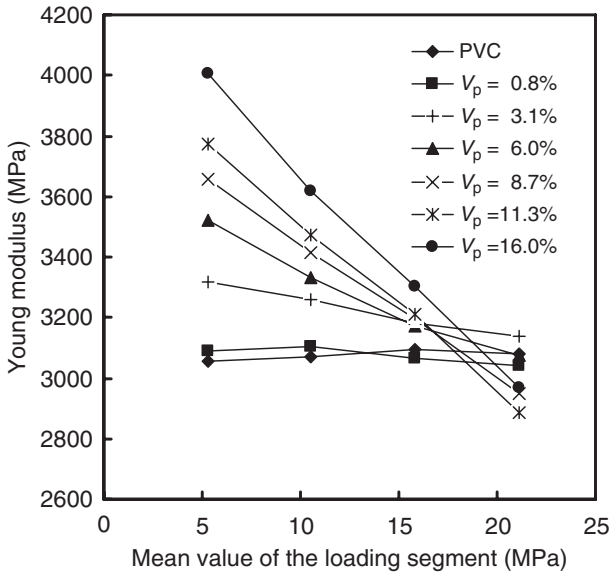

Figure 6: Evolution of Young's modulus against loading segment mean value for different volume fractions

Figure 6 shows the variation of tangent modulus for room temperature (20 °C) calculated for several loading segments with 5.25 MPa of range, plotting E against the mean value of the loading segment. Figure 7 shows the same results but plotting in the ordinate axis the tangent modulus normalised with its initial value calculated for the lowest segment loading. A maximum value of 21 MPa for the mean value of the segment stress range was considered, which is distant enough from the plastic stress yielding of the matrix; Figure 3 shows that a minimum value of 60 MPa for the ultimate stress was obtained for the composite with the lowest resistance. It can be seen that for both PVC and PVC–$CaCO_3$ composite with 0.8% of volume fraction, tangent modulus is practically constant and independent of the segment loading value, putting in evidence that plastic yielding does not occur until the load level referred above. However, for the other volume fractions an important decrease of tangent modulus was observed when the load was increased during the flexural test, and also that this trend increases as the volume fraction is increased. For the higher volume fractions (V_p greater than 8.7%) tangent modulus decreases even below the PVC Young's modulus values.

Figure 8 represents a comparison of the experimental results for flexural elasticity modulus with the predictions made with some theoretical models suggested in the literature [3]. Only the results obtained at 20 °C were included in this analysis. Two series of experimental results were plotted corresponding to both extreme loading segments (mean segment stresses of 5.25 and 21 MPa). The tangent modulus values obtained for the lower loading segment stress are between the Reuss and Voigt predictions. However, for the higher loading segment tangent modulus tends to monotonically decreases with volume fraction, attaining values clearly below the matrix E modulus. Qiang Fu *et al.* [21] also found a similar behaviour for modified $CaCO_3$ particles in a matrix of high-density polyethylene (HDPE), although these authors did not make an extreme exhaustive analysis of the evolution of the elasticity modulus with the segment stress range. Modulus values of the composite E_c lower than the modulus of the matrix E_m were obtained by those authors for volume fractions

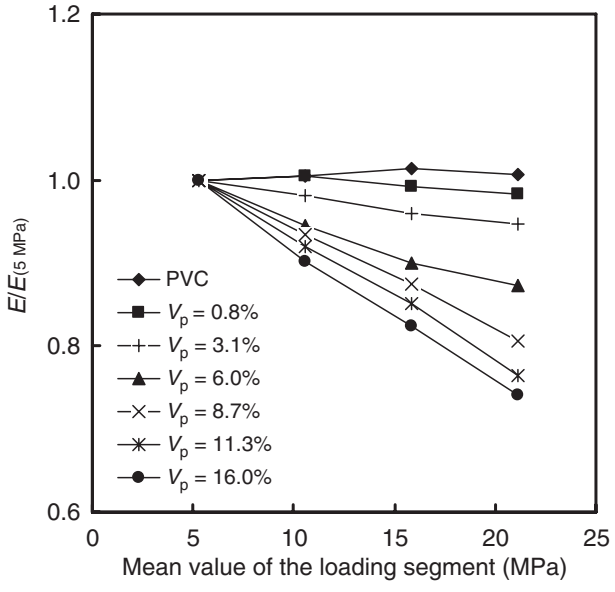

Figure 7: Evolution of normalised Young's modulus against loading segment mean value

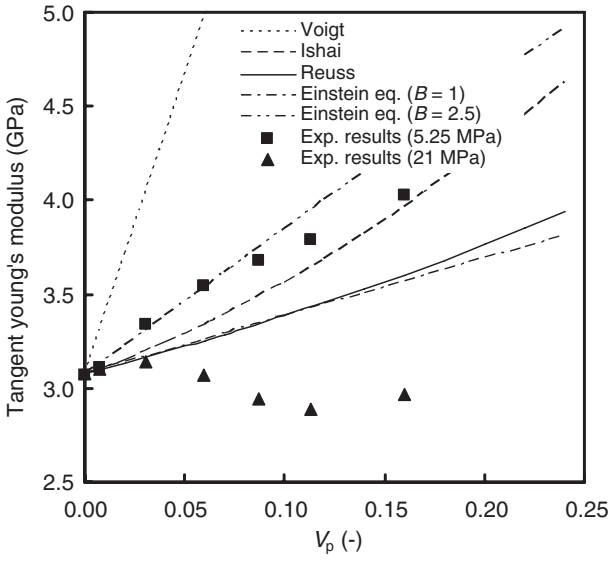

Figure 8: Comparison of the experimental results for E with some theoretical models

up to 10%, therefore below the predictions of the models giving lower bounds. They explain this behaviour through the softening of the interfacial layers caused by the treatment of the $CaCO_3$ particles with phosphate. Therefore, a flexible interfacial area having lower stiffness was expected in HPDE/$CaCO_3$ composites. Another factor that can contribute to this behaviour is one related with the interfacial adhesion. Most of the models dealing with the reinforcement action of the filler on the modulus assume that the adhesion is perfect between the filler and the matrix. Einstein's equation [3], which is applicable only for materials filled with low concentration of non-interactive spheres,

$$E_c = E_m(1 + BV_p) \tag{6}$$

was also plotted in Figure 8. If there is no adhesion between the filler and the matrix, we have $B = 1$, while for excellent adhesion between filler and interphase, we have $B = 2.5$. Experimental results obtained for the lower loading segment (5.25 MPa) are close the theoretical values of Einstein's equation with $B = 2.5$, indicating that the adhesion between PVC and $CaCO_3$ is initially good. However, for the higher loading segment (21 MPa) it can be seen that experimental results are below the theoretical values of Einstein with $B = 1$, indicating that there is no more adhesion between PVC and $CaCO_3$. Therefore, it seems that, initially, the adhesion exist but is weak, leading to a loss of the composite stiffness, for very low stresses, when adhesive breaks. In flexure tests, the specimens are submitted to a non-uniform stress distribution. Therefore, the stress plotted in Figures 6 and 7 is the maximum value of the flexure stress gradient. Considering that the observed decrease of Young's modulus with the increase of the applied load during the test is caused by a early debonding of the filler particles from the matrix, we can easily understand that this phenomenon did not occur simultaneously at all the specimen. Instead of this, it will grow from the most tensile-stressed layers of the specimen towards the flexure neutral axis. Consequently, it will occur a progressive and not to an abrupt decrease of the Young modulus. As the flexure load is increased, more particles will debond and act as holes. Sato and Furukawa [22] theoretically discuss the case of imperfect adhesion in the elastic regime, assuming that the non-bonding particles acted as holes and, therefore, predicted a decrease in modulus with increasing filler content. However, one can argue that the non-bonded particles do not behave entirely as holes, because they also restrain the matrix from collapsing. Another factor that can contribute to this effect concerns the thermal contraction stress at the particle–matrix interface. On cooling to T_g, PVC solidifies and begins to contract. Above T_g, stresses in the polymeric melt relax rapidly, but below T_g they do not. As thermoplastics have much higher coefficients of thermal contraction than $CaCO_3$, cooling to lower temperatures leads to clamping forces that are generated by differential thermal contraction. Although the interface might be shown as weak when tensile forces act perpendicularly to the surface, it is strong in shear because of friction.

To model this effect, that can contribute to the progressive decrease of the Young's modulus and the increase of the applied load, a simplified finite element analysis was carried out. A plane strain 2D model was considered. Figure 9 presents the geometry and finite element mesh for the composite, considering a circular particle with diameter ranging between 0.75 and 3.53 μm in a 7-μm square matrix, leading to a volumetric fraction ranging between 0.9 and 20%. The materials were assumed to be homogeneous, isotropic with linear elastic properties. The elastic properties considered were: E_{PVC} = 2690 MPa (20 °C) and E_{CaCO_3} = 35000 MPa [23]. Quadratic isoparametric elements were used. The model in Figure 9 has 640 elements in the matrix and 4800 elements in the particle for a total number of 16641 nodes. The particle and matrix were not glued but just in contact with a friction coefficient of 0.3. This model was submitted to compression to simulate the clamping forces that are generated by differential

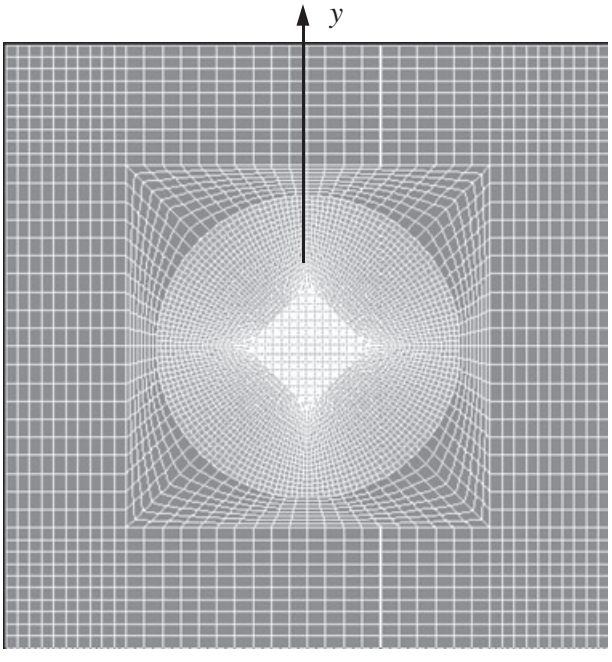

Figure 9: Geometry and finite element mesh for the composite model: a circular particle in a square matrix

© 2009 Blackwell Publishing Ltd | *Strain* (2011) **47**, e292–e304
doi: 10.1111/j.1475-1305.2009.00624.x

thermal contraction during cooling to temperatures below T_g. A fixed compressive displacement of 28×10^{-6} mm was imposed to all boundaries to simulate a temperature variation of 50 °C, assuming that the thermal expansion of PVC is about 80×10^{-6} m (m^{-1} °C^{-1}). Additionally, the top boundary was submitted to vertical displacement Y and reaction force at the bottom boundary was measured. Young's modulus was obtained dividing reaction stress by vertical strain. Figure 10 shows the variation of the Young's modulus with Y displacement for four different values of the filler volume fraction. It can be observed that for low values of Y displacement E increases with volume fraction. However, after some Y threshold value E decreases quickly, reaching a relatively low value and, finally, E remains constant. It can be also observed that as the volume fraction is increased a greater reduction of E is obtained, leading to final E-values that are in an opposite relative position in comparison with its initial values. For the lower volume fraction of 0.9%, the Young's modulus remains approximately constant and equal to the matrix E-value. The influence of the clamping forces that are generated by differential thermal contraction during cooling was also analysed and depicted in Figure 11 for the 10% volume fraction and two differential temperatures: ΔT = 50 and 25 °C. The Figure shows that the initial and final values of E do not depend of the clamping forces value, but the Y displacement threshold value tends to increase as the clamping forces increase as a result of higher differential thermal contraction. In general, it can be concluded that the model adopted in the numerical analysis gives results with the same trends that were observed experimentally, i.e. the progressive decrease of the Young's modulus as the load is increased and its dependence relatively to the volume fraction. Therefore, these numerical results increase the confidence in the explanation proposed.

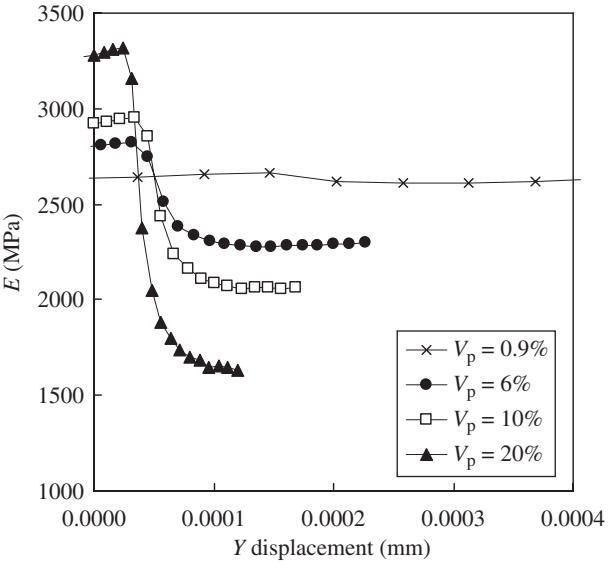

Figure 10: FE simulation of the Young's modulus variation with Y displacement for four different values of the filler volume fraction

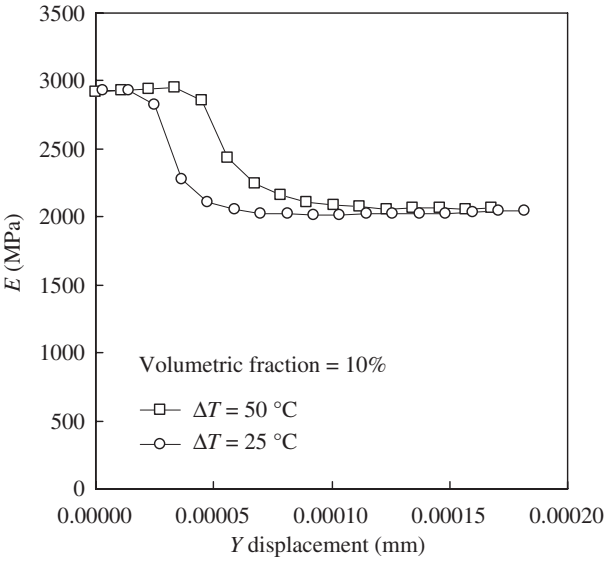

Figure 11: FE simulation on Young's modulus variation with Y displacement for two different values of clamping forces – volume fraction = 10%

The occurrence of an eventual high level of voids associated to an imperfect processing of the composite was also verified, leading to the conclusion that it was not observed a significant level of voids that could influence the values of the Young's modulus. As we can observe in Table 3, the density of the composites for the range of volume fractions analysed is always above the matrix density and in agreement with the expected calculated values, based on the volume fraction and the densities of the components. Density was measured according to the procedures described in ISO 1183 A [24].

Table 3: Comparison between measured and estimated densities of PVC/$CaCO_3$ composites

	Density		
V_p (%)	Measured	Estimated	Error (%)
0	1.32	1.32	–
0.8	1.37	1.33	2.92
1.6	1.38	1.34	2.90
3.1	1.42	1.36	4.23
6.0	1.45	1.41	2.76
8.7	1.49	1.45	2.68
11.3	1.50	1.48	1.33
16.0	1.55	1.55	0.00

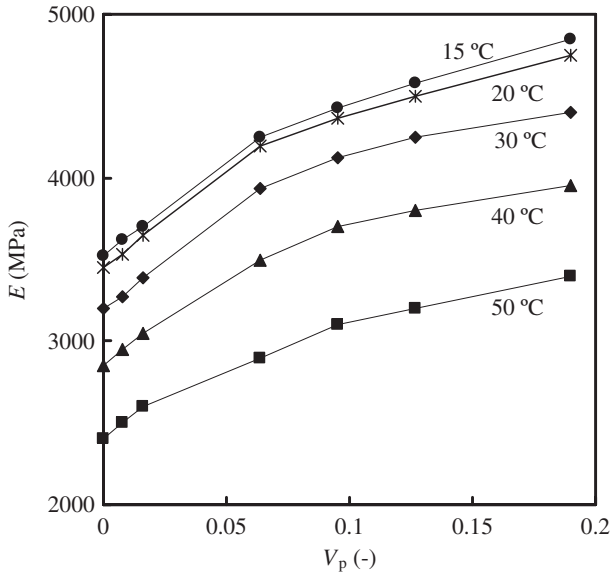

Figure 12: Young's modulus obtained by the resonant technique for different temperatures as function of volume fraction

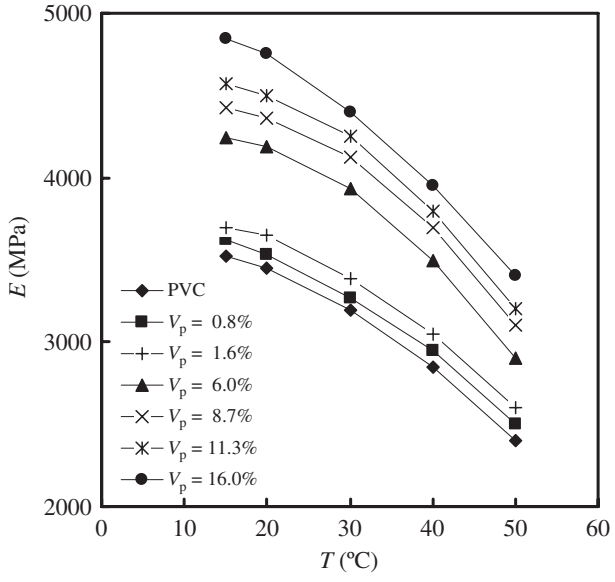

Figure 13: Young's modulus obtained by the resonant technique for different volume fractions as function of temperature

Resonant technique tests

Figure 12 shows the variation of Young's modulus with temperature (15, 30, 40 and 50 °C), against volume fraction for $CaCO_3$ filler with a particle size of 2.5 μm. These *E*-values were determined by the resonant technique described before. The trends observed are similar to those obtained in the flexure tests: (i) a significant decrease on Young's modulus with the increase of temperature; (ii) a monotonic increase of Young's modulus with volume fraction for the five temperatures analysed ranging between 15 and 50 °C. Figure 13 shows the same results but

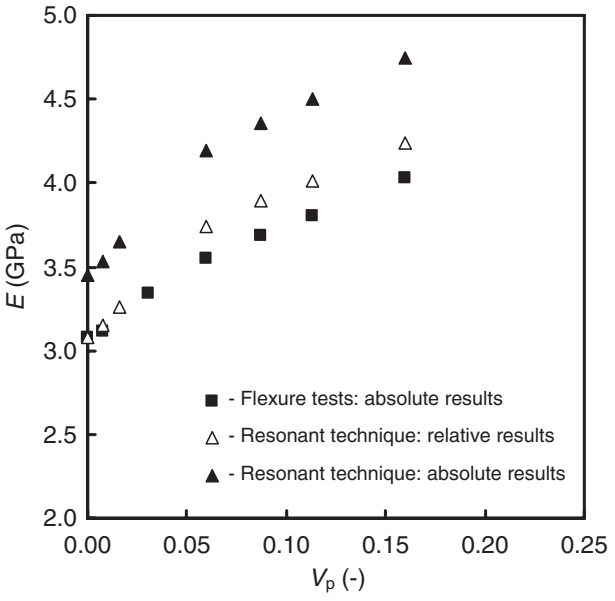

Figure 14: Comparison of Young's modulus obtained by both flexural tests and resonant technique

plotting *E* against the temperature for the seven values of volume fraction analysed shows it to range between 0 and 16%. In general, the results present a more consistent dependence of *E* with the variables analysed (temperature and volume fraction) because of three reasons: (i) the same specimen of each volume fraction was used for all temperatures, as this technique provides a non-destructive test; (ii) the vibration signal is a global response of the specimen, reducing statistical effects because of a non-homogeneous microstructure; (iii) a better control of temperature is provided by the oven used with this technique, without the inconvenience of great masses of the steel flexure testing supports being inside the oven.

Figure 14 compares the Young's modulus values obtained by the two techniques. Flexure data are the higher values depicted in Figure 6, i.e. the values obtained for the lower segment load with a mean stress of about 5.25 MPa. It can be observed that Young's modulus obtained by the resonant technique are greater (about 17% higher) than the *E* flexure test results. When normalising the resonant *E*-values to obtaining the coincidence of PVC *E*-values for both techniques, it can be observed that both series present the same trend with respect to the influence of the volume fraction and are even almost superimposed. It is reasonable to expect resonant *E*-values to be greater than flexural *E*-values because the resonant technique is a dynamical test while flexure test is a quasi-static test. To explain the different *E*-values obtained by the two techniques, additional 3P bending tests were carried out in a PVC specimen at room temperature and using several displacement rates: 0.01, 0.5, 2, 10,

© 2009 Blackwell Publishing Ltd | *Strain* (2011) **47**, e292–e304
doi: 10.1111/j.1475-1305.2009.00624.x

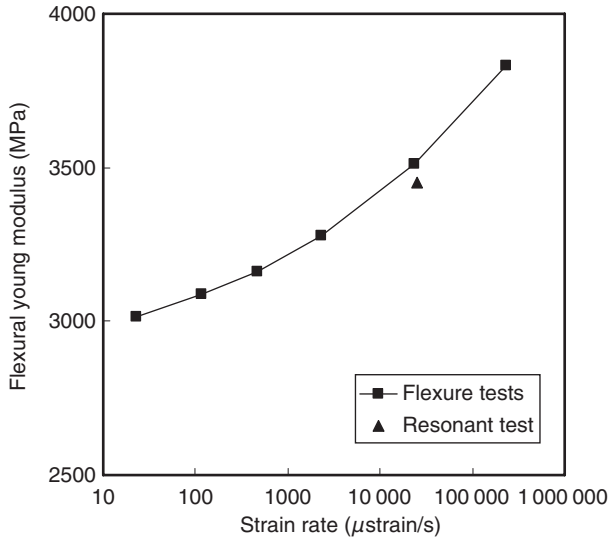

Figure 15: PVC Young's modulus against strain rate obtained in flexure tests and resonant technique. T = 20 °C

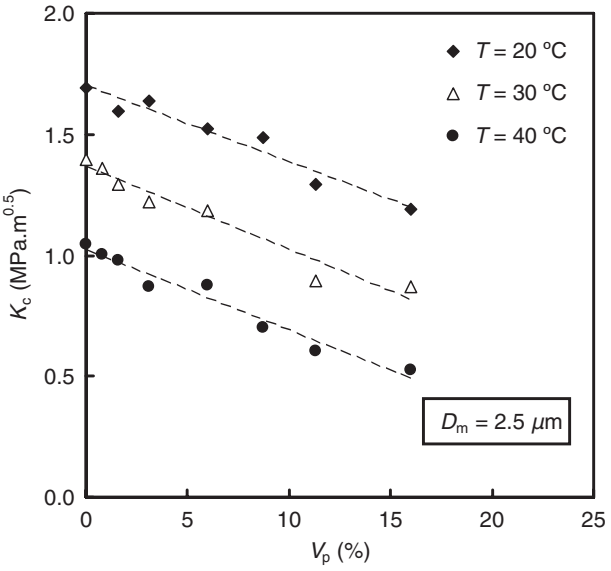

Figure 16: Fracture toughness K_c for different temperatures as function of volume fraction

100 and 1000 mm min^{-1}. Figure 15 shows Young modulus against strain rate calculated at the specimen middle section. The PVC E-value obtained with the resonant technique for T = 20 °C was also plotted in Figure 17 for comparison. Strain rate in the sample tested with the resonant technique was calculated using Equation (7):

$$\frac{d\varepsilon}{dt} = \pi\sqrt{2}\varepsilon_a f \tag{7}$$

where f is the resonant frequency and ϵ_a is the average value of the strain amplitude measured during resonant test. Despite the lower level of strains involved in the resonant technique, the high values (above 500 Hz) obtained for the resonant frequencies, leads to strain rates of more than two orders of magnitude above the value used in the E flexural tests plotted in Figure 14.

Figure 15 shows that PVC is a very sensitive material to strain rate. It is also observed a reasonable agreement between E-values by the two techniques when strain rate is taking into account.

Greater Young's results in the resonant test by comparison with the flexural test were also obtained by Ramalho *et al.* [25] for a polyester–silica particulate composite with 5.65 μm particle size and volume fractions ranging between 0 and 46%. However, the difference observed in their work was not as high as in this study. In the case of metals, the same authors [15] observe a very good agreement between the E-values obtained through these two techniques when testing the specimens with the same equipment used in this work. Besides, there is a good agreement between E-values obtained by these authors and the well-accepted values referred in literature. The agreement between Young's modulus values obtained with the two techniques for materials, as metals, which have a very low strain rate sensitivity, leads to the conclusion that the differences observed in the E-values of PVC/$CaCO_3$ composites must be attributed to the different material behaviour (sensitivity to strain rate) in both conditions of testing, as shown in Figure 15.

Fracture toughness tests

Figure 16 shows the variation of fracture toughness with temperature (20, 30 and 40 °C), against volume fraction for $CaCO_3$ filler with a particle size of

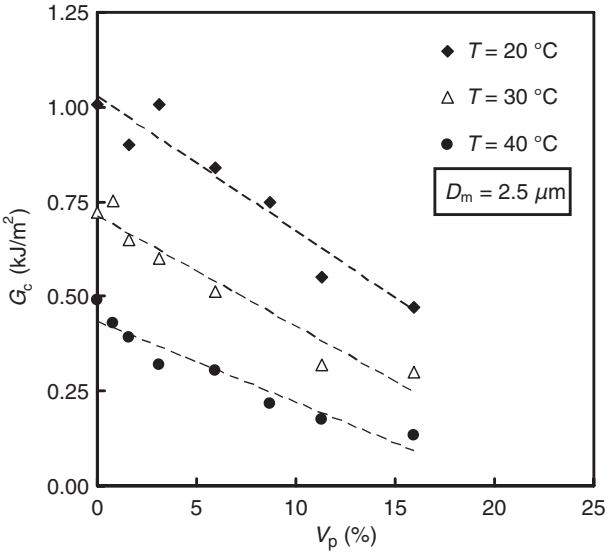

Figure 17: Fracture toughness G_c for different temperatures as function of volume fraction

2.5 μm. An important decrease of K_c was obtained with temperature increase, which is also the trend observed in the flexural strength tests. For the three temperatures, K_c shows a great and similar trend to decrease with filler volume fraction. A decrease of more than 0.5 MPa $(m)^{1/2}$ (about 25% for T = 20 °C) of toughness was observed when the volume fraction was increased from 0 to 16%.

Figure 17 shows the results obtained for the fracture energy G_c at 20, 30 and 40 °C. An important decrease of G_c with temperature increase was also obtained. For the three temperatures, an even greater decrease of G_c than the one observed for K_c was observed with the increase of particle volume fraction. For T = 20 °C a decrease of more than 50% on the fracture energy was observed when the volume fraction was increased from 0 to 16%. The fracture toughness can be related with the type of crack propagation modes: a discontinuous stick–slip type releases higher fracture energy than a continuous type. Only the continuous type crack propagation mode was observed in our tests. It was also reported in Ref. [26] that for 1–30 μm untreated glass beads a continuous crack propagation was observed up to 40% of the volume fraction. For larger beads (177–354 μm), the mode of crack propagation was a discontinuous stick–slip type.

Quiang Fu [20] divides the impact fracture of HPDE/$CaCO_3$ into three models, i.e. cavitation/crazing, cavitation and shear yielding coexisting, and matrix yielding, according to the surface-to-surface interparticle distance. He has reported that when the $CaCO_3$ weight fraction is less than 20–25%, the surface-to-surface interparticle distance is larger than a critical value, the fracture mode is by cavitation and crazing and the fracture is brittle. Above this weight fraction, the mode of fracture changes to ductile by cavitation and shear yielding and by matrix yielding. The observations by SEM for tests conducted at room temperature (20 °C) indicate that, at low volume fractions, the fracture is planar, of the brittle type

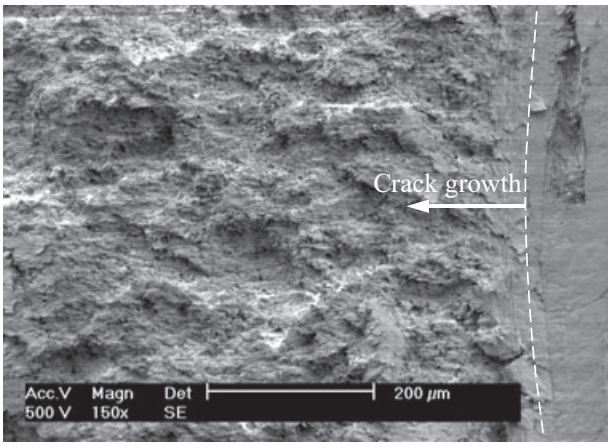

Figure 19: Fracture surface on a PVC/$CaCO_3$ specimen with V_p = 16%, D_m = 2.5 μm, T = 20 °C

(Figure 18A) and progresses from right to left. The surface appears to show a number of parabolas with the focus nearest the notch, which would indicate secondary crack fronts, each initiated from a single point, and overtaken by the main crack front from the introduced notch.

No great difference was observed between the aspect of this fracture surface and the one for PVC without filler (Figure 18B), except some cavitation visible from the particle locations. Figure 19 concerns a volume fraction of 16% and the same particle size. Now, we can observe a very different aspect of this surface of fracture, which appears to have an enormous number of secondary initiation sites.

Despite this, the fracture toughness obtained was very low, as discussed before, in terms of both K_c and G_c. We must conclude from the poor results obtained in this work, both in the flexural strength and fracture tests, that there is a bad adhesion between the filler and the matrix. It is desirable, in future research with these materials, that $CaCO_3$ particles are treated in an appropriate mode to improve its mechanical properties.

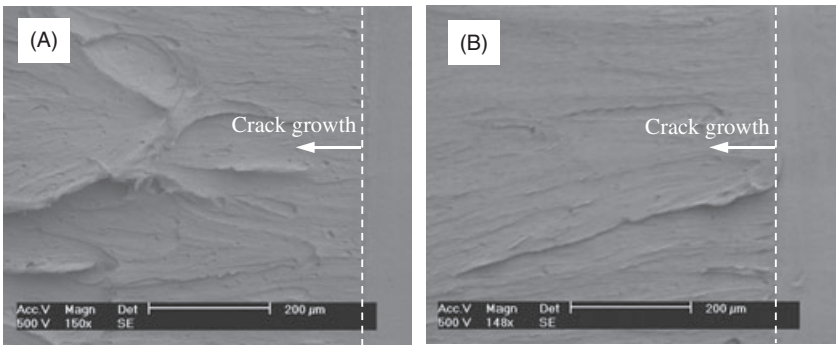

Figure 18: (A) Fracture surface on a PVC/$CaCO_3$ specimen with V_p = 0.8%, D_m = 2.5 μm, T = 20 °C; (B) fracture surface on a PVC specimen

doi: 10.1111/j.1475-1305.2009.00624.x

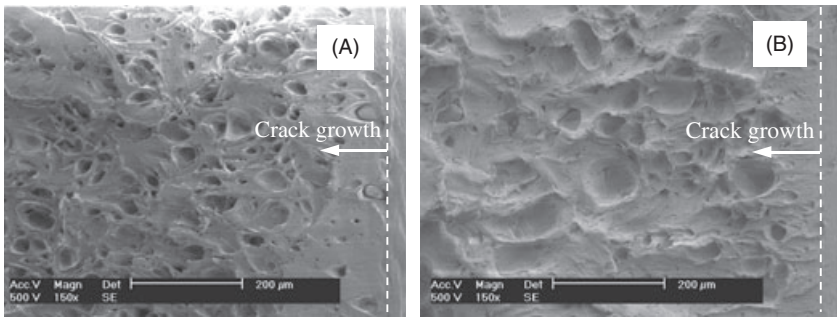

Figure 20: (A) Fracture surface on a PVC/$CaCO_3$ specimen with V_p = 6%, D_m = 23 μm, T = 20 °C; (B) fracture surface on a PVC/$CaCO_3$ specimen with V_p = 6%, D_m = 30 μm, T = 20 °C

To understand the influence of particle size on the fracture toughness, some exploratory tests were also carried out on specimens with greater particle size. For the same volume fraction, a slight reducing of fracture toughness with particle size was observed. Figure 20A concerns a volume fraction of 6% and a particle size of 23 μm, while Figure 20B illustrates a particle size of 30 μm. Evidence of weak interface can be clearly observed in both figures, allowing us to perceive that PVC is completely debonded from $CaCO_3$ particles by interface breaking. No fractured particles are observable. Some particles are visible at their original locations, revealing a clean surface, i.e. without the presence of a PVC layer. We can also see some large circular holes whose diameter is much wider than 30 μm. These are almost certainly because of plastic void expansion following debonding at the particle–matrix interface. On a microscopic scale, the failure is very ductile. However, void formation and expansion only confer an improvement of the level of macroscopic toughness on the composite if followed by orientation hardening. In these filled PVC specimens, it is immediately followed by fracture: local heating might probably have reduced the rate of strain hardening, leading to low-energy ductile fracture on the reduced load-bearing cross-section. The decreases of both flexural strength and fracture toughness with increasing filler content are caused by a correspondent increase in stress concentration and reducing of load-bearing cross-section.

Conclusions

Young's modulus, ultimate strength and K_c properties of PVC-based composite with $CaCO_3$ fillers were obtained for different weight fractions and temperatures. Significant decreasing on ultimate strength, fracture toughness and Young's modulus was observed with the increase of temperature. At room temperature, ultimate strength decreases with the increase of particle volume fraction.

PVC/$CaCO_3$ flexural Young's modulus calculated for a very lower loading segment increases with volume fraction. The same trend was obtained using the resonant technique. However, as the loading segment used to calculate the Young's modulus is increased a significant decrease of Young's modulus is obtained as a result of progressive debonding at the particle–matrix interface. This dependence of Young's modulus relatively to the loading segment increases as the volume fraction is increased, leading to composite Young's modulus below matrix value for higher volume fractions and higher loading segments. A simplified FE simulation also confirms such trend.

For the tested temperatures, a significant decrease of fracture toughness was observed with particle weight fraction. An insufficient adhesion between the particles and the matrix can be the cause for the poor results obtained in strength, stiffness and fracture toughness.

ACKNOWLEDGEMENT

The authors wish to thank the Cotrapla-Leiria company for providing the material used in the tests.

REFERENCES

1. Ferreira, J. A., Costa, J. D. and Capela, C. (1997) Fracture assessment in kitchen sinks manufactured with the PMMA/Si acrylic casting dispersion. *Theor. Appl. Fract. Mech.* **29**, 105–116.
2. Rothon, R. N. (2003) *Particulate-Filled Polymer Composites*. Rapra Technology Limited, Shawbury. ISBN 85957-382-7.
3. Ahmed, S. and Jones, F. R. (1990) A review of particulate reinforcement theories for polymer composites. *J. Mater. Sci.* **25**, 4933–4942.
4. Chen, N., Wan, C., Zhang, Y. and Zhang, Yinxi. (2004) Effect of nano-$CaCO_3$ on mechanical properties of PVC and PVC/Blendex blend. *Polym. Test.* **23**, 169–174.
5. Voros, G. and Pukanszhy, B. (1995) Stress distribution in particulate filled composites and its effect on micromechanical deformation. *J. Mater. Sci.* **30**, 4171–4178.

6. Pukanszky, B., Maurer, F. H. J. and Boode, J. W. (1995) Impact testing of polypropylene blends and composites. *Polym. Eng. Sci.* **35**, 1962–1971.
7. Jackson, A. P. J. and Vincent, F. V. (1990) Comparison of nacre with other ceramic composites. *J. Mater. Sci.* **25**, 3173–3178.
8. Liu, Z. and Gilbert, M. (1996) Structure and properties of talc-filled polypropylene: effect of phosphate coating. *J. Appl. Polym. Sci.* **59**, 1087–1098.
9. Chiu, H. T. and Chiu, W. M. (1996) Influence of mechanical properties in carbon black (CB) filled isotactic polypropylene (iPP) and propylene-ethylene block copolymer. *J. Appl. Polym. Sci.* **61**, 607–612.
10. Vollenberg, P. H. and Heikens, D. (1986) *Proceedings of the International Conference*. Fillers 86, Paper 14. PRI, London.
11. Liang, J. Z. and Li, R. K. Y. (1998) Mechanical properties and morphology of glass bead-filled polypropylene composites. *Polym. Compos.* **19**, 698–703.
12. Moloney, A. C., Kaush, H. H. and Stieger, H. R. (1983) The fracture of particulate-filled epoxid resins, Part 1. *J. Mater. Sci.* **18**, 208–216.
13. Zeng, X. F., Wang, W. Y., Wang, G. Q. and Chen, J. F. (2008) Influence of the diameter of $CaCO_3$ particles on the mechanical and rheological properties of PVC composites. *J. Mater. Sci.* **43**, 3505–3509.
14. Lauwagie, T., Sol, H., Heylen, W. and Roebben, G. (2004) Determination of the in-plane elastic properties of the different layers of laminated plates by means of vibration testing and model updating. *J. Sound Vib.* **274**, 529–546.
15. Antunes, F., Ramalho, A., Ferreira, J., Capela, C. and Reis, P. (2008) Determination of elastic properties by resonant technique: a sensitivity analysis. *J. Test. Eval.* **36**, 89–99.
16. American Society for Testing and Materials (1983) *Standard Test Methods for Flexural Properties of Unreinforced and Reinforced Plastics and Electrical Insulating Materials [Metric]*. ASTM, Annual Book of ASTM; Volume 08.01:ASTM D790M. West Conshobocken.
17. American Society for Testing and Materials (2006) *Standard Test Method for Dynamic Young's Modulus, Shear Modulus and Poisson's Ratio by Impulsive Excitation of Vibration*. ASTM, ASTM E1876-01. West Conshobocken.
18. EGF Task Group on Polymers and Composites. (1988) *A Linear Elastic Fracture Mechanics (CEFM) Standard for determining* K_c and G_c for Plastics. Testing protocol for Kc/Gc Standard. EGF Task Group on Polymers and Composites. London.
19. Nicolais, L. and Nicodemo, L. (1973) Strength of particulate composites. *Polym. Eng. Sci.* **13**, 469.
20. Bigg, D. M. (1987) Mechanical-properties of particulate filled polymers. *Polym. Compos.* **8**, 115–122.
21. Qiang, F., Guiheng, W. and Chunxiao, L. (1995) Polyethylene toughened by $CaCO_3$ particles: the interface behaviour and fracture mechanism in high density polyethylene/$CaCO_3$ blends. *Polymer* **36**, 2397–2401.
22. Sato, Y. and Furukawa, J. (1963) A molecular theory of filler reinforcement based upon the conception of internal deformation. *Rubber Chem. Technol.* **36**, 1081.
23. Wypych, G. (1999) *Handbook of Fillers*, 2nd edn. Plastics Design Library William and Andrew Inc, Toronto/New York.
24. International Standard Organization (1987) *Plastiques – Méthodes four déterminer la masse volumique et la densité relative des plastques nom alvéolaires*. ISO 1183 A 1987 (F). ISO, Geneva.
25. Ramalho, A., Antunes, P. V., Carvalho, M. D., Gil, H. and Rocha, J. (2006) Mechanical properties of particle reinforced resin composites. *Mater. Sci. Forum* **514–516**, 619–623.
26. Lange, F. F. and Radford, K. C. (1971) Fracture energy of a epoxy composite. *J. Mater. Sci.* **6**, 1197–1203.

doi: 10.1111/j.1475-1305.2009.00624.x